National Conference with International Participation
ENGINEERING MECHANICS 2006
Svratka, Czech Republic, May 15 – 18, 2006
paper no. 162

POST-IMPACT COMPRESSIVE LOAD CARRYING CAPACITY OF FIBRE-METAL LAMINATE PLATES

V. Obdržálek[*†], **J. Klement**[‡], **J. Vrbka**[*]

Summary: *Compression buckling and postbuckling behaviour of fibre-metal laminate plates with a single delamination has been investigated in order to estimate the compressive load carrying capacity of such plates. Drop-weight impact tests were performed to induce delaminations in fibre-metal laminate plates and subsequent ultrasonic inspection provided the contours of delaminated regions. These shapes of delaminations together with circular delamination shape were employed in the following finite element simulations of compressively loaded delaminated plates. Two load-limiting events were considered: yielding of metal layers and delamination growth initiation. It was found, that delaminations were not likely to grow before the onset of plastic deformation. The effect of delamination shape and buckling mode shape on the energy release rate values is also discussed.*

1. Introduction

Laminate structures have been more frequently used for primary aircraft structures, such as empennage, fuselage, wing skin etc. In order to design efficient yet safe structures, it is necessary to get insight into the failure processes in laminates and introduce the knowledge into the design process.

From all the possible failure modes of laminates, delamination – separation of laminate layers – seems to be the most dangerous and most common. Because the existence of delaminations in laminates can not be avoided, as they can form as a result of a low-velocity impact on laminate, the behaviour of delaminated composite structures has been under extensive investigation. It has been shown, that delaminations can significantly reduce both the buckling load and compressive load carrying capacity of laminated composite plates. However, buckling of a delaminated structure usually does not result in its immediate failure. On contrary, the failure load can be much higher than the buckling load. Therefore, it is desirable to investigate the effect of delamination upon the the postbuckling response of laminate structures.

Most studies into the delamination buckling of laminated composite plates with embedded delaminations focused on the behaviour of plates with delaminations of idealised shapes such as circular, rectangular or elliptical. Moreover, only some of these works examined delamination growth initiation and/or delamination growth:

Whitcomb (1989a) applied the virtual crack closure technique (VCCT) (Rybicki and Kanninen (1977)) to compute energy release rate along the front of circular delamination and pointed out, that the third

[*]Institute of Solid Mechanics, Mechatronics and Biomechanics, Faculty of Mechanical Engineering, Brno University of Technology, Technická 2, Brno 616 69, Czech Republic

[†]*Email address:* obdrzalek@fme.vutbr.cz

[‡]Institute of Aerospace Engineering, Faculty of Mechanical Engineering, Brno University of Technology, Technická 2, Brno 616 69, Czech Republic

mode energy release rate component ,$\mathcal{G}_{\mathrm{III}}$, is negligible. However, Whitcomb utilised a thin-film model assumption which may have influenced the results. The thin film model is based on the idea, that when one of the sublaminates is much thicker than the other one, it will not buckle. In the subsequent works Whitcomb (1989b, 1992) extended his analysis to elliptical delaminations and studied the effect of interpenetration of delaminated sublaminates upon the energy release rate distribution along the delamination front. Krüger et al. (1996) presented distributions of Mode I and Mode II energy release rate along the front of circular and elliptical delaminations. Suemasu et al. (1998a,b) investigated postbuckling behaviour of a plate with multiple circular delaminations. However, these works lack some important results related information and therefore the presented results are of limited value. Riccio et al. (2001) studied how geometrical parameters of a circular delamination may affect its growth initiation. Growth initiation of a circular delamination was also discussed by Singh et al. (2000) who, inter alia, studied the the effect of biaxial loading upon the value of mode I energy release rate.

Nilsson et al. (1993) studied the growth of a circular delamination. Like Whitcomb, Nilsson utilised the thin-film model assumption. The growth of the delamination was simulated by mesh moving technique. The Crack growth criterion was based on the stress intensity factors. Later on, Nilsson and Giannokopoulos (1995) extended their research to study the growth of a circular delamination with sinusoidal delamination front imperfections and load ratio imperfections. Finally, Nilsson et al. (2001) investigated the growth of a circular delamination, this time without the thin film model restriction.

Klug et al. (1996) analysed the delamination growth initiation of a circular and elliptical delamination and simulated the growth of the circular delamination by mesh moving technique. Unlike Nilsson, Klug's crack growth criterion was based only on the value of the total energy release rate. Shen et al. (2001), who also studied growth of a circular delamination, found that crack evolution criteria based on components of the strain-energy release rate predicted the rate of delamination growth much better than evolution criteria based on the total strain energy release rate. Shen also pointed out, that full plate model should be used to study the delamination growth. Xie and Biggers (2006a) developed algorithm based on VCCT to trace a moving delamination front with arbitrary shape. This approach was used to study the growth of a through-the-width, octagonal and square delamination (Xie and Biggers, 2006b). Cohesive interface elements were employed by de Moura et al. (2000) to study growth of a peanut shaped delamination.

Thomson and Scott (2000) and Armentani et al. (2004) studied the buckling and postbuckling behaviour of stiffened panels with a circular delamination positioned under the stiffener and presented energy release rate distributions along the delamination front. Yap et al. (2004) examined behaviour of a stiffened panel with rectangular and elliptical skin delamination and rectangular skin-stiffener delamination in various in-plane and out-of-plane positions and with different orientations and aspect ratios.

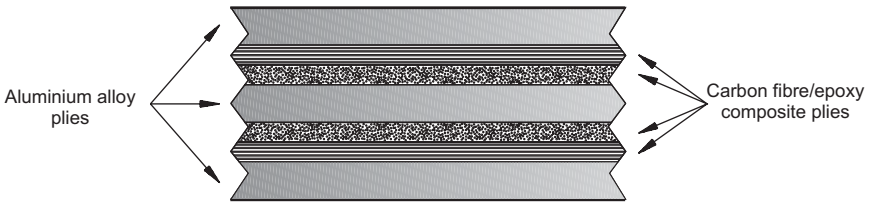

Figure 1: Example of a fibre-metal laminate

The present study is concerned with the analysis of the postbuckling behaviour of fibre-metal laminate plates with impact induced delamination. First of all, an experimental study into the shape of impact induced delamination in fibre-metal laminate plates was conducted. The shapes of delaminations were determined by ultrasonic inspection of fibre-metal laminate specimens which had been subjected to the impact loading with various impact energy levels. Non-linear finite element analyses were than performed in order to determine the compressive load carrying capacity of the plates. According to the well known fact, that the failure of a laminate structure with delamination structure is usually preceded by

limited delamination growth, the delamination growth initiation was considered to be the load limiting event. In addition, yielding of the metal layers was also concidered to be inadmissible, since residual deformation of laminate structures is often thought to be undesirable.

The outlined study into the behaviour of plates with delaminations of the shape that matches the shape of impact induced delaminations was limited only to several cases of the plates analysed in the experimental study. Therefore, in order to get greater insight into the phenomenon of delamination buckling, additional analyses of compressive strength of plates with circular delaminations were performed. These analyses focused on how the size of delamination and its through-the-thickness position may influence the the post-impact compressive strength of plates.

2. Experiment

The aim of the experimental study was to determine the shapes of impact induced delaminations in fibre-metal laminate plates. Twelve laminate specimens with dimensions of $130\times130\times1.83$ mm were prepared. Six specimens had Al/0/0/Al/0/0/Al layup and the other specimens had Al/0/90/Al/90/0/Al lauyp, where Al denotes metal layers and 0 or 90 denotes the orientation, θ, of unidirectional carbon fibre/epoxy composite plies with respect to the loading direction - see Figures 1 and 4.

All the specimens were than subjected to impact loading in a drop-weight impact machine. The specimens were positioned between the clamping plates with central circular window, which had a diameter of 80 mm. The striker had a hemispherical tip with a diameter of 12.7 mm and the weight of the striker was 2 kilograms. The impact energies of the striker were chosen to be 3 J, 6 J and 9 J. Two specimens for every unique combination of lay-up and impact energy were tested. The impacted specimens were than inspected by nondestructive ultrasonic technique to obtain the shape of induced delaminations. Results of the experiments are summarised in Table 1 and Figure 2.

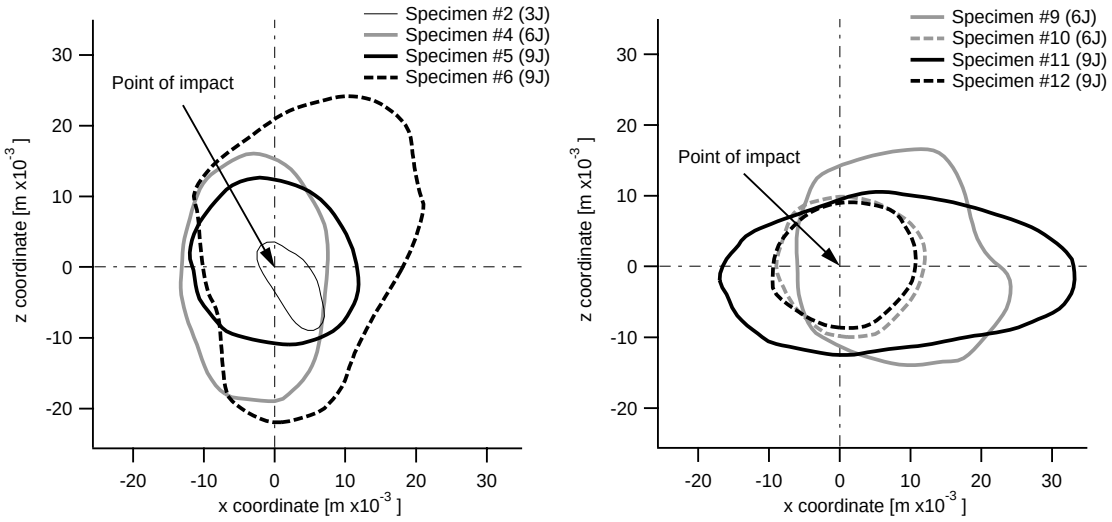

(a) Layup:Al/0/0/Al/0/0/Al (b) Layup:Al/0/90/Al/90/0/Al

Figure 2: Delaminated areas.

As it can be seen in Figure 2, there is some correlation between the value of impact energy and the size of delamination; however, some of the delaminations induced at an impact energy level of 6 J were larger than delaminations induced at an impact energy level of 9 J . This discrepancy is to be attributed to the way the ultrasonic inspection was carried out. As the inspection was done by a hand-held ultrasonic transducer, the results of such analysis highly depended on the test personell. Nevertheless, it can be seen,

that the specimens with cross-ply layup have different orientation of delaminations than the specimens with unidirectional layup.

Table 1: Delaminated areas.

Layup	Al/0/0/Al/0/0/Al						Al/0/90/Al/0/90/Al					
Specimen No.	1	2	3	4	5	6	7	8	9	10	11	12
Impact energy [J]	3	3	6	6	9	9	3	3	6	6	9	9
Delaminated area [mm^2]	-	69.0	NA	579.1	436.2	1059.4	-	-	706.2	321.1	859.8	280.7

3. Numerical analysis

Finite element analyses of the postbuckling behaviour of fibre-metal laminate plates with delaminations were performed using the ABAQUS finite element software package.

As already suggested, two types of delaminations were considered - circular delaminations and delaminations of shapes that matched the shapes of impact induced delaminations determined in the experimental study. The latter delaminations will be in the following text entitled as impact induced like delaminations (IIL delaminations).

Plates with IIL delaminations were modelled with the same layups as the specimens in the experimental study. Delaminations were assumed to exist between the first and second ply (A interface - see Table 2), since it is the most probable position. Plates with circular delamination were modelled with unidirectional layup (Al/0/0/Al/0/0/Al) and two variants of cross-ply layup (Al/0/90/Al/90/0/Al and Al/90/0/Al/0/90/Al). Circular delaminations were positioned at the A, B and C interfaces (Table 2), so all the possible positions were captured. All the plates were modelled with dimensions of $80\times80\times1.83$ mm.

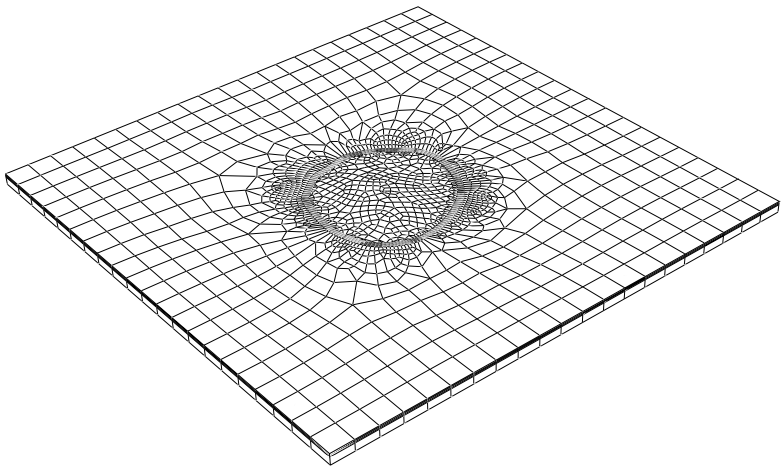

Figure 3: Finite element mesh

Four layers of eight-node multilayer continuum shell element were used to built the finite element mesh. Two layers of elements constituted the upper sublaminate and two layers the lower sublaminate. Elements were refined along the boundary of the delaminated area in order to achieve greater accuracy. Special effort was made to ensure the orthogonality of element edges lying along the delamination boundary so it was possible to use the virtual crack closure method to compute the release rates (Smith and Raju, 1998; Krueger, 2002). A typical finite element mesh is shown in Figure 3.

Table 2: Structure of the laminate.

Layer	thickness [mm]	interface
aluminium	0.4	A
composite	0.1575	B
composite	0.1575	C
aluminium	0.4	D
composite	0.1575	E
composite	0.1575	F
aluminium	0.4	

Material properties of the aluminium and composite plies are summarised in Table 3 and 4, respectively. Material of the composite layers was assumed to be orthotropic linear elastic and the constitutive model of metal layers was chosen to be elasto-plastic with isotropic hardening. The choice of the elasto-plastic material model, however, was thought to be too restrictive, because it is be impossible to use the virtual crack closure technique to compute the energy release rate once plastic deformation has developed. Consequently it would be impossible to study the load carryin capacity of common laminates which, unlike fibre metal laminates, are composed of composite materials that exhibit more or less linear elastic behaviour. Therefore, in order to obtain some information about the compressive strength of these common laminates, every plate configuration was also analysed with the constitutive model of the metal layers set to be isotropic linear elastic.

Table 3: Material properties of metal plies. True plastic strains ε_{pi} and corresponding Cauchy stressses σ_{yi} are used to define behaviour of the material in the elasto-plastic region.

2024 T6 aluminium alloy	
$E = 0.725$ GPa	$\nu = 0.34$
$\sigma_{y1} = 360$ MPa	$\varepsilon_{p1} = 0.000$
$\sigma_{y2} = 521$ MPa	$\varepsilon_{p2} = 0.077$

Contact conditions were employed to prevent inadmissible interpenetration of elements in the delaminated region. In order to promote the buckling of the plate, imperfection was introduced by inclusion of a virtual interference between plies at the delaminated region. The interference magnitude was chosen to be 1.10^{-6} m.

Table 4: Material properties of composite plies.

Hexcel unidirectional carbon/epoxy prepreg		
$E_{11} = 126.0$ GPa	$E_{22} = 11.0$ GPa	$E_{33} = 11.0$ GPa
$\nu_{12} = 0.28$	$\nu_{13} = 0.28$	$\nu_{23} = 0.40$
$G_{12} = 6.60$ GPa	$G_{13} = 6.60$ GPa	$G_{23} = 3.93$ GPa

Boundary conditions are shown in Figure 4. All the plate edges were assumed to be clamped. Compressive load was applied to the plate by uniform displacing of one of the edges.

The Newton-Raphson solution technique was employed to solve the non-linear postbuckling problem. Stabilization algorithm was used to overcome divergence problems which are interrelated with stability

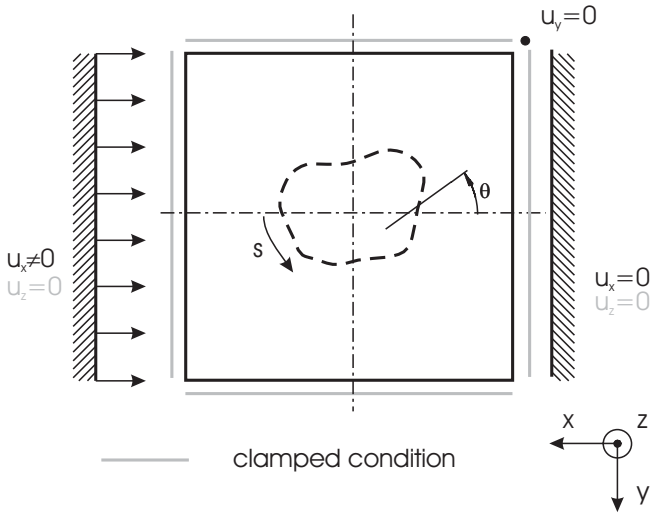

Figure 4: Boundary conditions.

problems. Once the finite element analysis run had finished, thevirtual crack closure technique was used to determine distributions of energy release rate components along the delamination front.

4. Results

In order to interpret the results in the following section correctly, it is desirable to address the issues of the buckling load and elastic limit load definitions first:

When the nonlinear buckling problem is solved, it is always difficult to identify the buckling load. In this work the buckling load was defined to be the load at the moment when the maximum deflection of the plate exceeded value of 5.10^{-6} m. Buckling loads determined by this simple method agreed well with the buckling loads obtained by a more rigorous method based on the construction of tangents to the load-deflection curve before and after the initial change of the slope of this curve. However, it is necessary to note, that the former method was slightly inaccurate when the initial buckling mode shape was the global one.

Unlike the problem of finding the buckling loads, the problem of finding the elastic limit loads is seemingly trivial. However, the moment of the onset of plastic deformation depends to some extent on the element mesh density. Therefore, all the presented values that correspond to the moment just before the onset of plastic deformation should be considered to be approximative. Nevertheless, since the size of elements along the plate boundaries and along the delamination front was approximately the same in all simulations, the results are comparable.

Table 5: Comparison of the normalised buckling loads P_{cr} and elastic limit loads P_{pl}. P_{cr}^{nondel} is the buckling load of a plate withou delamination.

	Al/0/0/Al/0/0/Al $P_{cr}^{nondel} = 49525$ N				Al/0/90/Al/0/90/Al $P_{cr}^{nondel} = 49245$ N			
Specimen No.	2	4	5	6	9	10	11	12
P_{cr}/P_{cr}^{nondel}	1.00	0.90	0.82	0.44	0.41	0.80	0.35	0.89
P_{pl}/P_{cr}^{nondel}	1.00	0.98	0.91	0.67	0.57	0.84	0.48	0.91

4.1 Plates with impact induced like delamination

Summary of the buckling loads, P_{cr}, and elastic limit loads, P_{pl}, is presented in Table 5. It is evident, that the existence of delaminations may reduce the load carrying capability of laminate plates by more than 50 %.

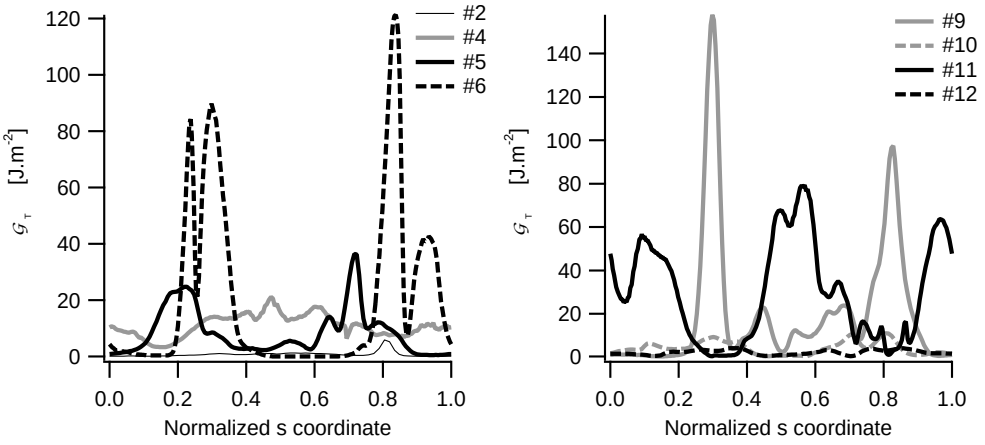

(a) Specimens No. 2,4, 5 and 6. (b) Specimens No. 9,10, 11 and 12.

Figure 5: Distributions of totat energy release rate along the delamination front at the moment just before the onset of plastic deformation.

Distributions of the total energy release rate, $\mathcal{G}_{\mathrm{T}} = \mathcal{G}_{\mathrm{I}} + \mathcal{G}_{\mathrm{II}} + \mathcal{G}_{\mathrm{III}}$, along the delamination front for all the analysed cases are compared in Figures 5 and 6. In Figure 5 are plotted $\mathcal{G}_T$ distributions at the the moment just before the onset of plastic deformation. Summary of the maximum values of the total energy release rate is also presented in Table 6. It can be seen, that none of the delaminations is expected to grow, because the interlaminar fracture toughness is likely to be greater than $140\,\mathrm{J.m^{-2}}$.

Table 6: Comparison of the maximum values of the totat energy release rates, $\mathcal{G}_{\mathrm{T}}$ [J.m^{-2}] (arabic numbers), buckling mode shapes and dominant components of the $\mathcal{G}_{\mathrm{T,max}}$ (roman numbers). Plates with impact induced like delamination. Description of the buckling mode shapes: L – local, G – global, M – mixed, U – U shape, N – unbuckled

Layup	Al/0/0/Al/0/0/Al				Al/0/90/Al/0/90/Al			
Specimen No.	2	4	5	6	9	10	11	12
onset of	5.9	21.1	36.4	121.4	157.9	11.0	79.4	4.2
pl. deform	GU;II	GU;I	L;I	L;I	L;I,II	L;I	L;II,I	N;I,II
$P = 40\,\mathrm{kN}$; linear elastic	6.0	0	0	319.5	781.9	1.7	767.5	0
behaviour of metal layers	N	N;I	N	MU;I	MU;I,III	N;I	MU;II,I	N

In Figure 6 are plotted distributions of the total energy release rate, $\mathcal{G}_{\mathrm{T}}$, along the delamination front at load $\mathrm{P} = 40\,\mathrm{kN}$ (linear elastic constitutive behaviour of metal plies). Maximum values of the total energy release rate are summarised in Table 6. It can be seen, that plates with cross-ply lay-up are likely to have lower load carrying capability than plates with unidirectional lay-up.

4.2 Plates with circular delamination

Summary of the normalised buckling loads, $\mathrm{P_{cr}}$, and elastic limit loads, $\mathrm{P_{pl}}$ is presented in Tables 7 and 8, respectively. It can be seen, that the closer the delaminations were to the plate surface and the larger

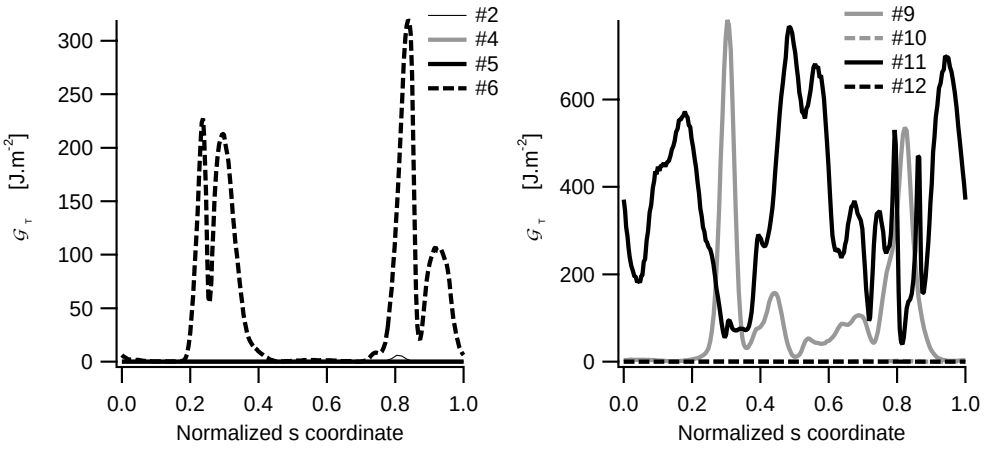

(a) Specimens No. 2,4, 5 and 6. (b) Specimens No. 9,10, 11 and 12.

Figure 6: Distributions of the totat energy release rate, $\mathcal{G}_{\mathrm{T}}$, along the delamination front for $P = 40\,\mathrm{kN}$; linear elastic behaviour of aluminium layers.

they were, the smaller the buckling and elastic limit loads were observed. In no case the elastic limit load preceded the buckling load.

Table 7: Comparison of the normalised compressive buckling loads $\mathrm{P_{cr}/P_{cr}^{nondel}}$. Plates with circular delamination. $\mathrm{P_{cr}^{nondel}}$ is buckling load of a plate without delamination.

		Al/0/0/Al/0/0/Al $\mathrm{P_{cr}^{nondel}} = 49525$ N			Al/0/90/Al/90/0/Al $\mathrm{P_{cr}^{nondel}} = 49245$ N			Al/90/0/Al/0/90/Al $\mathrm{P_{cr}^{nondel}} = 48710$ N		
	Delaminated interface	A	B	C	A	B	C	A	B	C
Delamination diameter [mm]	ø20	0.98	0.98	0.99	0.85	0.94	0.99	0.85	0.98	1.00
	ø30	0.51	0.62	0.79	0.37	0.47	0.77	0.38	0.63	0.86
	ø40	0.28	0.36	0.47	0.21	0.27	0.47	0.21	0.36	0.57
	ø50	0.18	0.23	0.31	0.13	0.18	0.31	0.14	0.24	0.37

Table 8: Comparison of the normalised compressive loads $\mathrm{P_{cr}/P_{cr}^{nondel}}$ at the moment just before the onset of plastic deformation. Plates with circular delamination. $\mathrm{P_{cr}^{nondel}}$ is buckling load of a plate without delamination.

		Al/0/0/Al/0/0/Al $\mathrm{P_{cr}^{nondel}} = 49525$ N			Al/0/90/Al/90/0/Al $\mathrm{P_{cr}^{nondel}} = 49245$ N			Al/90/0/Al/0/90/Al $\mathrm{P_{cr}^{nondel}} = 48710$ N		
	Delaminated interface	A	B	C	A	B	C	A	B	C
Delamination diameter [mm]	ø20	1.00	1.00	1.00	0.88	0.98	1.00	0.89	0.99	1.00
	ø30	0.71	0.85	0.89	0.55	0.66	0.82	0.56	0.71	0.86
	ø40	0.61	0.69	0.73	0.48	0.55	0.64	0.47	0.55	0.70
	ø50	0.54	0.58	0.68	0.42	0.46	0.57	0.41	0.53	0.64

Summary of the maximum values of the total energy release rate, $\mathcal{G}_{\mathrm{T}}$, is presented in Tables 9 and 10. Values in the former table correspond to the moment just before the onset of plastic deformation and the latter table comprises of data which correspond to the moment when the compressive load reached value of approximately $40\,\mathrm{kN}$ (linear elastic constitutive behaviour of metal layers).

Unlike impact induced like delaminations, large circular delaminations near the mid-plane of the plate

Table 9: Comparison of the maximum values of the total energy release rate $\mathcal{G}_{\mathrm{T}}$ [J.m^{-2}] (arabic numbers), buckling mode shapes and dominant energy release rate components of $\mathcal{G}_{\mathrm{T,max}}$ at the moment just before the onset of plastic deformation (roman numbers). Plates with circular delamination. Description of buckling mode shapes: L – local, G – global, M – mixed, U – U shape

Layup		Al/0/0/Al/0/0/Al			Al/0/90/Al/90/0/Al			Al/90/0/Al/0/90/Al		
Delaminated interface		A	B	C	A	B	C	A	B	C
Delamination diameter [mm]	ø20	4.1 GU;II	7.8 GU;II	9.0 GU;II	6.8 L;I	7.5 MU;II,I	0.9 GU;II	7.5 l;II	1.4 GU;I,II	0.3 GU;II
	ø30	59.8 L;I	60.3 L;I,II	19.3 MS;II,III	69.0 L;I	69.4 L;II,I	34.8 MS;III,I	70.5 L;I,II	40.7 L;I	12.6 GS;III
	ø40	115.3 L;I	139.0 L;I,II	97.8 L;II,I	119.8 L;I	152.8 L;II,I	159.5 L;I,II	109.1 L;I,II	123.6 L;I	60.2 MS;I,III
	ø50	131.3 L;I	163.1 L;I,II	225.2 L;II,I	131.7 L;I	175.2 L;I,II	290.9 L;I,II	117.3 L;I,II	247.8 L;I	155.8 MU;II,I

Table 10: Comparison of the maximum values of the total energy release rate, $\mathcal{G}_{\mathrm{T}}$ [J.m^{-2}] (arabic numbers), buckling mode shapes and dominant energy release rate components of $\mathcal{G}_{\mathrm{T,max}}$ (roman numbers). Plates with circular delamination subjected to compressive load of approximately 40 kN. Elastic behaviour of metal layers. Description of the buckling mode shapes: G – global, M – mixed, U – U shape, S – S shape, N – unbuckled.

Layup		Al/0/0/Al/0/0/Al			Al/0/90/Al/90/0/Al			Al/90/0/Al/0/90/Al		
Delaminated interface		A	B	C	A	B	C	A	B	C
Delamination diameter [mm]	ø20	0.0 N	0.0 N	0.0 N	0.0 N	0.0 N	0.0 N	0.0 N	0.0 N	0.0 N
	ø30	133.0 MU;I	41.2 MU;I,II	1.4 N;II,I	412.0 MU;I	224.9 MU;II,I	20.1 GS;I,III	431.7 MU;I,II	168.1 MU;I	0.0
	ø40	435.4 MU;I,II	321.8 MU;I,II	544.7 MS;III	880.5 MU;I	1226.8 MS;III,I	1206.8 MS;III	919.1 MU;I,II	878.0 MS;I,III	767.5 MS;III
	ø50	713.9 MU;I	692.9 MU;I,II	872.2 MS;III	1236.6 MU(S);I	1688.9 MS;III,I	1675.5 MS;III	1205.4 MU(S);I,III	1236.7 MU(S);I,III	1062.8 MS;II

may start to grow even before the onset of plastic deformation.

A closer look at Tables 7 and 8 reveals dependence of the dominant components of the maximum total energy release rate on the buckling mode shape. When there was a gap between the delaminated sublaminates, mode I energy release rate component usually prevailed. Global buckling mode shapes (Figures 7(a) and 7(b)) featured dominant shearing energy release components of $\mathcal{G}_{\mathrm{T,max}}$ - mode II component in case of U-like shape and mode III component in case of S-like shape. Mixed mode shapes (Figures 7(c) and 7(d)), which are somewhat halfway between the local and global modes, were mostly characterised by a combination of dominant mode I and mode II or III components, depending on the prevailing U- or S-like shape of plate. Discrepancies between the outlined relationships and actual values presented in the Tables 6, 7 and 8 should be mainly attributed to the difficulty in distinguishing one buckling mode from another (e.g. see Figure 7(e)).

It should be also pointed out, that mode III energy release rate component of $\mathcal{G}_{\mathrm{T,max}}$ became dominant only when significant loads were applied.

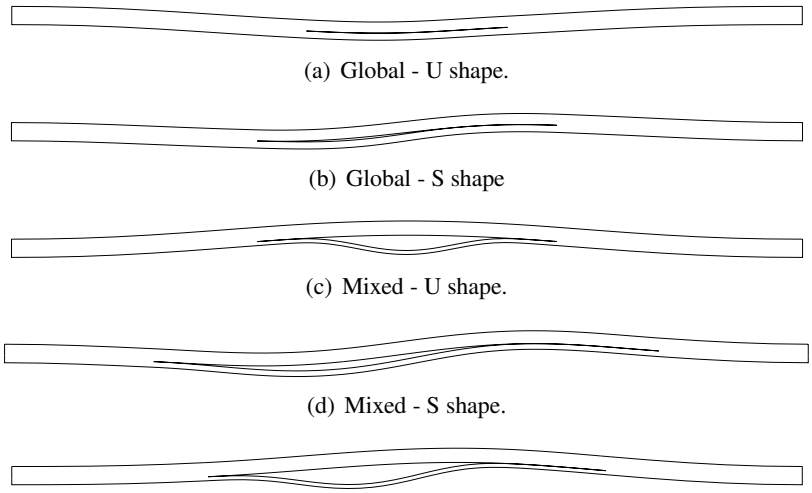

(a) Global - U shape.

(b) Global - S shape

(c) Mixed - U shape.

(d) Mixed - S shape.

(e) Mixed - U shape; transition to S shape.

Figure 7: Buckling mode shapes.

4.3 Comparison of limit loads vs. delamination shape

Idealisation of the shape of impact induced delamination with circular shape may greatly simplify the analysis of the post-impact strength of laminates. Therefore, it is interesting to compare the behaviour of plates with IIL delaminations to the behaviour of plates with circular delaminations.

Four out of the eight delaminations identified in the experimental study were large enough to reduce the compressive load carrying capacity of plates which contained near surface delamination of the same shape. Those four delaminations were found in specimens no. 4,6,9 and 11. As it can be seen in Table 11, plates with one of these IIL delaminations exhibited greater elastic limit loads than plates with circular delamination at the same depth, with similar maximum dimension and in plates with the same layup. Similar conclusion, however, can not be made when the maximum values of the total energy release rate, $\mathcal{G}_{\mathrm{T,max}}$, at the moment just before the onset of plastic deformation are considered. Looking again at Table 11, it can be seen, that the $\mathcal{G}_{\mathrm{T,max}}$ value corresponding to the plate with delamination of the same shape as delamination identified in the specimen no. 9 is greater than $\mathcal{G}_{\mathrm{T,max}}$ value corresponding to the plate with circular delamination of similar size as the IIL delamination. Although this is the only case of the four considered, it should be concluded that models of plates with circular delaminations should not be used to investigate the compressive strength of plates with impact induced like delaminations.

Table 11: Comparison of the maximum values of the total energy release rate, $\mathcal{G}_{\mathrm{T}}$ [J.m^{-2}] and normalised elastic limit loads $\mathrm{P_{pl}}$. $\mathrm{P_{cr}^{nondel}}$ is the buckling load of a plate without delamination. Plates with IIL delaminations and plates with circular delaminations.

Layup	Al/0/0/Al/0/0/Al				Al/0/90/Al/0/90/Al			
Specimen No.	4		6		9		11	
Diameter [mm]		ø40		ø50		ø30		ø50
$\mathrm{P_{pl}/P_{cr}^{nondel}}$	0.98	0.61	0.67	0.54	0.57	0.55	0.48	0.42
$\mathcal{G}_{\mathrm{T,max}}$ [J.m^{-2}]	21.1	115.3	121.4	131.3	157.9	69.0	79.4	131.7

5. Conclusions

Non-linear finite element analyses of compressively loaded fibre-metal laminate plates with delamination of circular shape and the shape that matched the shape of impact induced delamination were performed. Issue of the oad carrying capacity of delaminated plates was addressed. Two limiting events were considered: onset of plastic deformation of metal layers and delamination growth initiation.

The results can be summarised as follows:

- Delaminations of the shape that matched the shape of impact induced delaminations were unlikely to start to grow before the onset of plastic deformation. However, this conclusion may not be true for large circular delamination near the mid-plane of a plate.
- Laminated plates with cross-ply lay-up possesed lower load carrying capacity than plates with unidirectional layup.
- For each plate buckling mode shape was typical different dominant energy release rate components that constitute the maximum total energy release rate $\mathcal{G}_{\mathrm{T}}$ found along the delamination front: local buckling mode shape – mode I, mixed buckling mode shape – mode I and II or III, U-like global buckling mode shape, S-like global buckling mode shape – mode III.
- Because S-like global buckling mode shape of plates was only observed in case of plates loaded beyond the elastic limit load, it is not necessary to measure the mode III interlaminar fracture toughness of fibre-metal laminates.
- Models of plates with circular delaminations should not be used to predict the postbuckling behaviour of plates with impact induced delaminations, because delamination growth initiation may not be predicted correctly.

6. Acknowledgement

Support from the Faculty od Mechanical Engineering BUT under grant BD 1353019 is gratefully acknowledged. Moreover, the first author would like to express gratitude to V. Pavelka from Faculty of Chemistry BUT for help with experiments.

7. References

Armentani, E., Caputo, F., Esposito, R. and Godono, G. (2004), Evaluation of energy release rate for delamination defects at the skin/stringer interface of a stiffened composite panel, *Engineering Fracture Mechanics* **71**, pp. 885–895.

de Moura, M. F. S. F., Gonçalves, J. P. M., Marques, A. T. and de Castro, P. M. S. T. (2000), Prediction of compressive strength of carbon-epoxy laminates containing delamination by using a mixed-mode damage model, *Composite Structures* **50**, pp. 151–157.

Klug, J., Wu, X. X. and Sun, C. T. (1996), Efficient modelling of postbuckling delamination growth in composite laminates using plate elements, *AIAA Journal* **34**(1), pp. 178–184.

Krueger, R. (2002), The virtual crack closure technique: history, approach and applications, *Technical Report NASA/CR-2002-211628*, NASA Langley Research Center.

Krüger, R., Hänsel, C. and König, M. (1996), Experimental-numerical investigation of delamination buckling and growth, *Technical Report ISD-Report 96/3*, Institut für Statik und Dynamik der Luft- und Raumfahrtkonstruktionen, Universität Stuttgart.

Nilsson, K. F., Asp, L. E. and Sjörgen, A. (2001), On transition of delaminated growth behaviour for compression loaded composite panels, *International Journal of Solids and Structures* **38**.

Krüger, R., Hänsel, C. and König, M. (1996), Experimental-numerical investigation of delamination buckling and growth, *Technical Report ISD-Report 96/3*, Institut für Statik und Dynamik der Luft- und Raumfahrtkonstruktionen, Universität Stuttgart.

Nilsson, K. F., Asp, L. E. and Sjörgen, A. (2001), On transition of delaminated growth behaviour for compression loaded composite panels, *International Journal of Solids and Structures* **38**.

Nilsson, K. F. and Giannokopoulos, A. E. (1995), A finite element analysis of configurational stability and finite growth of buckling driven delamination, *Journal of the Mechanics and Physics of Solids* **43**(12), pp. 1983–2021.

Nilsson, K. F., Thesken, J. C., Sindelar, P., Giannokopoulos, A. E. and Storåkers, B. (1993), A theoretical and experimental investigation of buckling induced delamination growth, *Journal of the Mechanics and Physics of Solids* **41**(4), pp. 749–782.

Riccio, A., Scaramuzzino, F. and Perugini, P. (2001), Embedded delaminations growth in composite panels under compressive load, *Composites: Part B* **32**, pp. 209–218.

Rybicki, E. F. and Kanninen, M. F. (1977), A finite element calculation of stress intensity factors by a modified crack closure integral, *Engineering Fracture Mechanics* **9**, pp. 931–938.

Shen, F., Lee, K. H. and Tay, T. E. (2001), Modeling delamination growth in laminated composites, *Composites Science and Technology* **61**, pp. 1239–1251.

Singh, K. L., Dattaguru, B., Ramamurthy, T. S. and Mangalgiri, P. D. (2000), Delamination tolerance studies in laminated composite panels, *Sādhanā* **25**(4), pp. 409–422.

Smith, S. A. and Raju, I. S.: 1998, Evaluation of stress-intensity factors using general finite element models, *in* T. L. Panontin and S. D. Sheppard (eds), *Fatigue and Fracture Mechanics: 29th Volume, ASTM STP 1321*, American Society for Testing and Materials, pp. 176–200.

Suemasu, H., Kumagai, T. and Gozu, K. (1998a), Compressive behavior of multiply delaminated composite laminates part 1: Experiment and analytical developement, *AIAA Journal* **36**(7), pp. 1279–1285.

Suemasu, H., Kumagai, T. and Gozu, K. (1998b), Compressive behavior of multiply delaminated composite laminates part 2: Finite element analysis, *AIAA Journal* **36**(7), pp. 1286–1290.

Thomson, R. S. and Scott, M. L. (2000), Modelling delaminations in postbuckling stiffened composite shear panels, *Computational Mechanics* **26**, pp. 75–89.

Whitcomb, J. D. (1989a), Predicted and observed effects of stacking sequance and delamination size in instability related delamination growth, *Journal of Composites Technology and Research* **11**(3), pp. 94–98.

Whitcomb, J. D. (1989b), Three-dimensional analysis of a postbuckled embedded delamination, *Journal of Composite Materials* **23**, pp. 862–889.

Whitcomb, J. D. (1992), Analysis of a laminate with a postbuckled embedded delamination, including contact effects, *Journal of Composite Materials* **26**(10), pp. 1523–1535.

Xie, D. and Biggers, S. B. (2006a), Strain energy release rate calculations for a moving delamination front of arbitrary shape based on the virtual crack closure technique. part I: Formulation and validation, *Engineering Fracture Mechanics* **73**, pp. 771–785.

Xie, D. and Biggers, S. B. (2006b), Strain energy release rate calculations for a moving delamination front of arbitrary shape based on the virtual crack closure technique. part II: Sensitivity study on modeling details, *Engineering Fracture Mechanics* **73**, pp. 786–801.

Yap, J. W. H., Thomson, R. S., Scott, M. L. and Hachenberg, D. (2004), Influence of post-buckling behaviour of composite stiffened panels on the damage criticality, *Composite Structures* **66**, pp. 197–206.